Geotech Geol Eng (2018) 36:3751–3766
https://doi.org/10.1007/s10706-018-0569-9

ORIGINAL PAPER

# Geomechanical Rock Properties Using Pressure and Temperature Dependence of Elastic P- and S-Wave Velocities

**Hem Bahadur Motra · Hans Henning Stutz**

Received: 21 March 2017 / Accepted: 4 May 2018 / Published online: 12 May 2018


**Abstract** It is important and meaningful for understanding the geomechanical properties of rock and providing guidance on analyzing and simulating the formation processes of engineering, geophysical, geothermal, civil and underground engineering projects. Variation in geomechanical properties of metamorphic rock, such as, seismic velocities (P-and S-wave) density deformation, is observed with the increase in pressure and temperature, Poisson's ratio, elastic modulus, bulk modulus and shear modulus, are analyzed herein. A simple laboratory method, which measure seismic velocities has increasingly been conducted to determine the geomechanical properties of rock materials. Three metamorphic rock samples were selected for laboratory testing. Laboratory testing were done on cube samples of dry rocks in a true triaxial apparatus. First, P and S wave velocities were measured at 12–100 MPa pressure and at 20–600 °C temperature. Measurement showed that P and S wave velocities increase with increasing pressure and decrease with increasing temperature. Second, the wave velocities are used to calculate the geomechanical properties at lower to higher pressure and temperature. Furthermore, it was found that pressure and temperature have a significant effect on the change of geomechanical properties of rocks. These results contribute to a reliable estimate of geomechanical properties of rocks.

**Keywords** Geomechanical rock properties · P and S wave · Anisotropy · Dynamic elastic moduli

**List of symbols**

| | |
|---|---|
| E | Young's modulus |
| k | Bulk modulus |
| $m_d$ | Dry mass |
| V | Volume |
| μ | Shear modulus |
| ρ | Density |
| $V_p$ | Compression wave velocity |
| $V_s$ | Shear wave velocity |
| ε | Deformation |
| ν | Poisson's ratio |

H. B. Motra (✉)
Marine and Land Geomechanics and Geotechnics, Institute of Applied Geo-Science, Christian-Albrechts-Universität, Ludewig-Meynstr. 10, 24118 Kiel, Germany
e-mail: hbmotra@gmail.com

H. H. Stutz
Department of Engineering - Geotechnical Engineering, Aarhus University, Inge Lehmanns Gade 10, Aarhus C, Denmark

## 1 Introduction

Reliable estimates of the geomechanical characteristics of rocks are required for almost any form of design and analysis used in various geomechanical projects such as mining, civil nuclear, waste disposal, geothermal energy and geotechnical engineering. Indeed, most of geomechanical projects can occur in metamorphic rocks basement. However, the geomechanical properties of such rocks remain poorly known compared to sedimentary rocks. The geomechanical properties of metamorphic reservoir rocks need to be even better understood. Rock deformation and failure or strength behavior are fundamental problems in geomechanics (Schön 2011). Physical characteristics of rocks include density, Poisson's ratio and elastic moduli. Rock geomechanical characteristics mainly include elastic modulus, Poisson's ratio, shear modulus, bulk modulus and rock strength. These parameters can be obtained from the measurement of seismic wave velocities of core samples from lab experiments. The change of pressure and temperature affect properties of the seismic wave velocities.

The seismic wave techniques are frequently used to determine the geomechanical properties of rocks. The seismic wave velocities [compressional wave P ($V_p$) and shear wave S ($V_s$)] can easily be determined by the laboratory method. The seismic waves of rock are closely related to the intact rock properties such as mineral, shape, density, porosity, anisotropy, pore water confining pressure, temperature, weathering and discontinuities (Lama and Vutukuri 1978). Numerous laboratory measurements have been performed to determine the pressure dependence of ultrasonic wave velocities in rocks (D'Andrea et al. 1966; Deere and Miller 1965; Youash 1970; Smorodinov et al. 1970; Kern 1978; Gebrande et al. 1982; Kern et al. 1997, 2001; Punturo et al. 2005; Moradian and Behnia 2009; Sarkar et al. 2012; Motra and Wuttke 2016). However, experiments focusing on the temperature dependence of ultrasonic wave velocities in rocks are rare. Changes in pressure and temperature alter the mineral composition and elastic properties of rocks (Tian et al. 2012; Hajpál and Török 2004). The effect of pressure and temperature on the physical and mechanical properties of rocks has been an important topic in rock mechanics because high pressure and temperature affect the thermal stress, mineral expansion, physical and mineralogical properties of rock (Kern et al. 1997; Tian et al. 2012; Hajpál and Török 2004; Liu et al. 2016; Tian et al. 2013; Nye 1985). Many studies were carried out of the pressure dependent physical and geomechanical properties of rocks e.g. density strength, tensile strength and Young's modulus.

A number of researchers have attempted to evaluate the pressure and temperature dependent characteristics of sand stone and sedimentary rocks. However, the theoretical investigation of the effect of high pressure and temperature on the geomechanical properties of metamorphic rock specimen through the seismic wave measurement remains unaddressed. In this work, we are interested to determine the geomechanical properties of the active geothermal area's metamorphic rock specimen.

## 2 Theoretical Background

The propagation of an elastic wave through an elastic medium can be described by the infinitesimally small deformations in the transmitted body responding to an external stress.

Pressure dependence seismic wave velocities [compressional P-wave ($V_p$) and shear S-wave ($V_s$)], which are closely linked to the elastic and geomechanical properties, can be determined using the ultrasonic pulse emission technique [e.g. Kern et al. 1997; D'Andrea et al. 1966; Deere and Miller 1965; Punturo et al. 2005; Moradian and Behnia 2009; Sarkar et al. 2012], few experiments have focused on the temperature dependence [e.g. Kern et al. 1997; Motra and Wuttke 2016; Motra and Zertani 2018] studied the characteristics of acoustic emissions during the deformation of different kinds of metamorphic rocks under true in situ conditions.

Hooke's Law states that for small elastic deformations, the strain that a deformed body experiences is linearly proportional to the applied stress which can be expressed mathematically as:

$$\sigma_{ij} = C_{ijkl}\varepsilon_{kl} \tag{1}$$

where $\sigma$ is the second-rank stress tensor. $C$ represents a fourth-rank tensor of elastic stiffness *(ijkl* = 1, 2, 3 indicate one of the three orthogonal axes) with 81 components and $\varepsilon$ is a second rank strain tensor

$$\varepsilon_{kl} = \frac{1}{2}\left(\frac{\partial u_k}{\partial x_i} + \frac{\partial u_i}{\partial x_k}\right) \tag{2}$$

where u is the displacement. The above equation can be further reduced from four indices *ijkl* down to two indices *mn* by introducing the Voigt notation (Nye 1985) and after conservation of energy considerations:

$$\begin{aligned} C_{ijkl} = C_{jikl} = C_{ijlk} = C_{jilk} = C_{mn}(i,j,k,l \\ = 1,2,3; m,n = 1,\ldots 6) \end{aligned} \tag{3}$$

which then simplify the generalized Hooke's Law into a matrix equation:

$$\sigma_I = c_{IJ}\varepsilon_J \tag{4}$$

The elastic stiffness tensor can be reduced from 81 to 36 independent components or elastic constants. Each $C_{IJ}$ is one of the components of a 6 × 6 symmetric matrix with the stiffness tensor reduces to 21 independent components that is symmetric about the diagonal:

$$\begin{pmatrix} \sigma_1 \\ \sigma_2 \\ \sigma_3 \\ \sigma_4 \\ \sigma_5 \\ \sigma_6 \end{pmatrix} = \begin{pmatrix} C_{11} & C_{12} & C_{13} & C_{14} & C_{15} & C_{16} \\ C_{21} & C_{22} & C_{23} & C_{24} & C_{25} & C_{26} \\ C_{31} & C_{32} & C_{33} & C_{34} & C_{35} & C_{36} \\ C_{41} & C_{42} & C_{43} & C_{44} & C_{45} & C_{46} \\ C_{51} & C_{52} & C_{53} & C_{54} & C_{55} & C_{56} \\ C_{61} & C_{62} & C_{63} & C_{64} & C_{65} & C_{66} \end{pmatrix} \begin{pmatrix} \varepsilon_1 \\ \varepsilon_2 \\ \varepsilon_3 \\ \varepsilon_4 \\ \varepsilon_5 \\ \varepsilon_6 \end{pmatrix} \tag{5}$$

which describes the stress–strain relations for a general anisotropic material such as that observed in a triclinic symmetry where the indices $I$ and $J$ are related to the $ij$ in according to the cyclical notation *I, J* =1, 2, 3, 4, 5, 6 when *ij* or *kl* = 11, 22, 33, 13 or 31, 23 or 32, 12 or 21 respectively.

For an isotropic material, the number of independent constants reduces to two and the tensor of elasticity has the form:

$$C_{IJ} = \begin{pmatrix} C_{11} & C_{12} & C_{12} & 0 & 0 & 0 \\ C_{21} & C_{11} & C_{12} & 0 & 0 & 0 \\ C_{12} & C_{12} & C_{11} & 0 & 0 & 0 \\ 0 & 0 & 0 & C_{44} & 0 & 0 \\ 0 & 0 & 0 & 0 & C_{44} & 0 \\ 0 & 0 & 0 & 0 & 0 & C_{44} \end{pmatrix} 0 \tag{6}$$

with $c_{12} = c_{11}–2c_{44}$. The relationship between the components and the Lame parameters $\lambda$, $\mu$ are:

$$c_{11} = \lambda + 2\mu, \quad c_{12} = \lambda, c_{44} = \mu, \tag{7}$$

Besides the Lame parameters $\lambda$, $\mu$, any pair of two of the following moduli can be used for a description of the elastic properties of an isotropic material.

However, if elastic wave velocities $V_p$ and $V_s$, respectively and bulk density $\rho$ are known from measurements, the elastic parameters can be calculated:

$$\mu = \rho \cdot V_s^2 \tag{8}$$

where $\mu$ is the shear modulus, $\rho$ is the bulk density and $V_s$ is the shear wave velocity. The dry density ($\rho$) was determined as following:

$$\rho = \frac{m_d}{V} \tag{9}$$

where $m_d$ is the weight of sample after drying and $V$ is volume of sample.

$$v = \frac{1}{2}\left(\frac{V_p^2 - 2V_s^2}{V_p^2 - V_s^2}\right) \tag{10}$$

where $v$ is the Poisson's ratio and $V_p$ is the compressional wave velocity.

$$\begin{aligned} E &= \rho \cdot V_p^2\left(\frac{(1+v)(1-2v)}{1-v}\right) \\ &= \rho \cdot V_s^2\left(\frac{3V_p^2 - 4V_s^2}{V_p^2 - V_s^2}\right) \end{aligned} \tag{11}$$

where $E$ is the Young's modulus.

$$k = \rho\left(V_p^2 - \frac{4}{3}V_s^2\right) \tag{12}$$

where $k$ is the bulk compressional modulus.

**Table 1** Sample overview: rock types, mineral contents and (micro-) structural features

| Sample | Rock type | Minerals | Structures and microstructures |
|---|---|---|---|
| A | Quartz Mica Schist | Qtz, Ms, Chl, Tur, Ilm, Zr | Fine grained, foliated with deformational structures; Abundant Calcite in crosscutting plagues and veins, porosity: 1% |
| B1/B2 | Amphibolite | Hbl, Bt, Qtz, Pl, Ap, | Small grain size, Hbl-prevailling levels 2–3 mm thick alternating with Bt + Qtz levels |

Rock samples, composition and (micro-) structural features

*Minerals-Ap*apatite, *Bt* biotite, *Chl* chlorite, *Hbl* hornblene, *Ilm* ilmenite, *Ms* muscovite, *Qtz* quartz, *Tur* turmaline, *Zr* zircon, *Pl* plagioclase

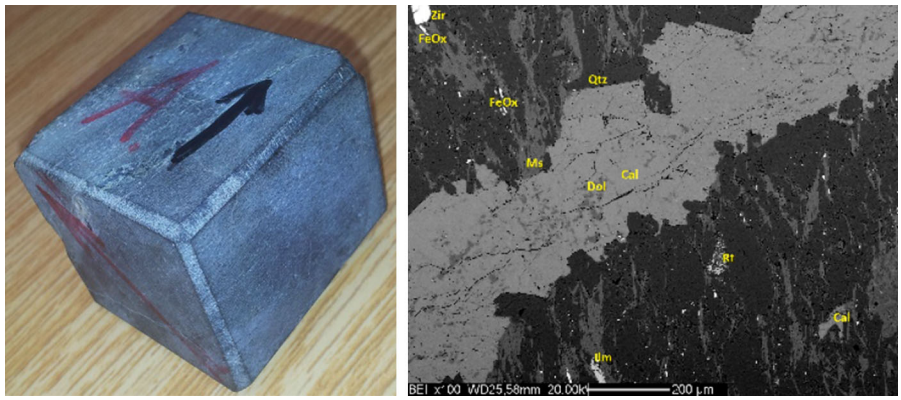


**Fig. 1** Sample and thin section of A

## 3 Rock Sample Characterization and Experimental Technique

### 3.1 Rock Sample Characterization

Table 1 gives an overview over sample locations, rock types, mineral contents and (micro-) structural features.

The investigated samples core sections can be described as follows:

The sample is part of the Torrente Mersino Quarzitic Formation. Figures 1 show A sample cubes with different reference systems. Figure 1 shows pictures of a thin section of this rock. It is a foliated, fine grained Quartz Mica Schist with strong deformational structures. Quartz is prevailing over muscovite. Accessory minerals are tourmaline, zircon, chlorite, ilmenite (FeOx), rutile and rare apatite with very small grain sizes. In addition, calcite occurs in large, to very large plaques made out of very large crystals and veins crosscutting the schistosity, often with Chlorite along the grain boundaries. The schistosity is planar with very close spacing (less than 1 mm) and marked by very thin layers of muscovite and opaques. Quartz grains with fish or rounded shapes are also present with larger sizes and unclear grain boundaries. Porosity is not visible in the thin section of this sample. Calcite occurs in crosscutting plagues and veins. Large crystals are also present.

Although the mineral composition of the sample selected for the experiments varies (Figs. 1, 2), they comprise very similar elemental compositions as obtained by X-ray fluorescence (XRF) analysis (Table 1), electron microscope scanning with micro-thin section studies carried out.

The sample B1/B2 was taken from approximately 3.28 km depth. The sample cubes of B1 and B2 are pictured in Fig. 2 which shows a thin section the sample. It is an Amphibolite with planar schistosity and small grain sizes, composed of hornblende, biotite, quartz and minor apatite, titanite and opaques. It has a strong foliation, a general small crystal grain size. Within the sample, alternating levels of either hornblende- dominated areas or quartz- biotite

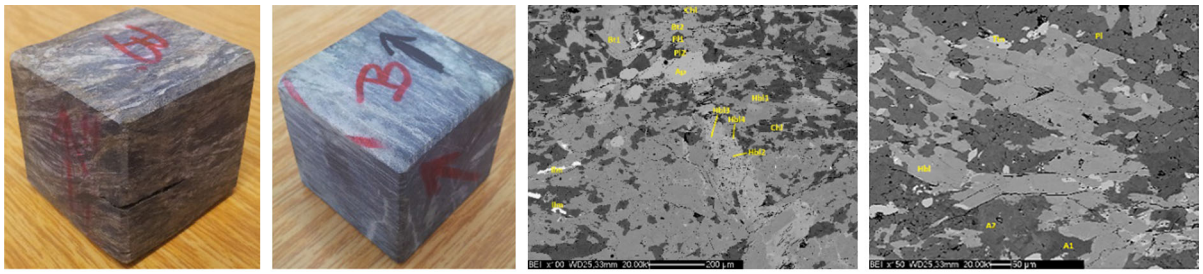


**Fig. 2** Sample and thin section of B1/B2

dominated areas of 3–4 mm thickness are visible. Hbl crystals can reach sizes of 2–3 mm and titanite crystals are also present in aggregates of many small crystals, elongated as the schistosity.

### 3.2 Experimental Technique

The elastic P- and S-wave velocities ($V_p$ and $V_s$) and the resulting velocity anisotropies of the investigated samples were determined experimentally using the ultrasonic pulse emission technique. The measurements were conducted on cube-shaped specimens (Fig. 3) in a true triaxial multi-anvil press that allows maximum pressure and temperature conditions of 150 MPa and 600 °C. A state of nearly isotropic stress was achieved by confining the sample cube with six pyramidal pistons. The arrangement of the sample-piston-transducer assembly allows simultaneous measurements of compressional Vp and the two orthogonally polarized shear wave velocities ($S_1$, $S_2$), each in three orthogonal directions of a sample cube (43 mm edge-length). The possibility to measure S1 and S2 allows for the extraction of the amplitude of shear wave splitting, which in itself is a measure for anisotropy (Kern et al. 1997; Punturo et al. 2005; Motra and Wuttke 2016; Scheu et al. 2006).

Measurements were carried out over a range of pressures up to 150/100 MPa (in situ condition) and temperatures up to 600 °C. The measurement procedure can be divided into two cycles. During the first cycle (pressure cycle), pressure is increased stepwise, starting with 12 MPa followed by 25, 35, 50, 75 and 100 MPa. Following that, the applied pressure is increased in steps of 50 MPa up to a maximum of

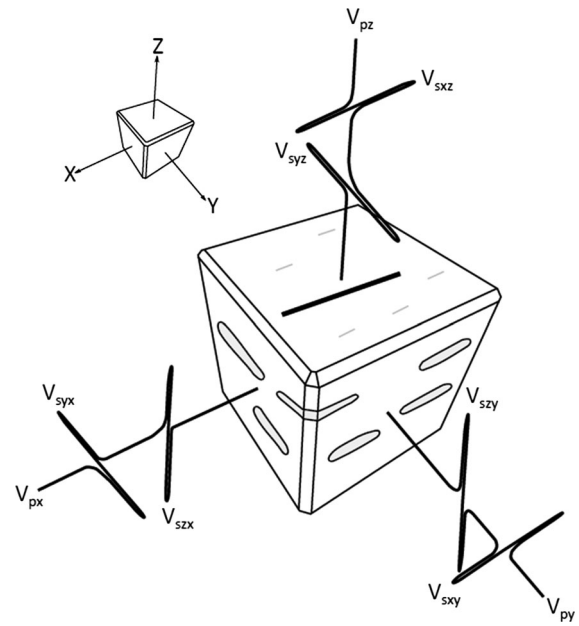


**Fig. 3** Representative illustration of a cube-shaped sample and its sample reference system as used during the experiments. X is parallel to the rocks lineation and Z is perpendicular to the foliation (X–Y plane) (Motra and Zertani 2018)

150 MPa. The temperature during this cycle remains at 20 °C.

During the second cycle (temperature cycle), pressure is constant at 150/100 MPa and temperature is increased stepwise with increment of 100 °C, respectively, until the maximum conditions of 600 °C are reached. At every step of the described two cycles, P- and S-wave velocities are measured to ensure that the influences of pressure and temperature can be analyzed independently. The heating rate

during the experiments is approximately 100 °C/30 min and it is necessary to maintain the temperature for 30 min in order to guarantee that all of the sample cube has a homogeneous temperature.

To measure the directional dependence of wave velocities (anisotropy), particularly in natural metamorphic rocks, which are generally anisotropic, the three orthogonal measuring directions must be related to the structural reference frame X, Y, Z, where Z is perpendicular and X and Y are parallel to the foliation (XY-plane). Further, X is parallel to the samples lineation (Fig. 3). Length changes (volume changes) of the samples as a function of pressure and temperature were obtained by measuring the piston displacements. A complete set of measured data comprises three P-wave velocities and six S-wave velocities obtained by determining the time it takes the wave to travel through the sample cube and the cube changes in length (volume changes). The sample-piston-transducer assembly is identical to the assembly used in Kern et al. (1997), Punturo et al. (2005), Motra and Wuttke (2016), D'Andrea et al. (1966) and the transducers operate at 2 MHz (P-wave) and 1 MHz (S-wave).

## 4 Results

### 4.1 Seismic Velocities

$V_p$- and $V_s$-wave velocities were measured simultaneously in the three structural directions. The rocks representing that thermally metamorphosed Schist with quartz prevailing on muscovite, pelitic schist, amphibolite. Three sleeted representative samples of that thermally metamorphosed rock (A, B1 and B2) for geomechanical measurements. Measurements were performed first at room temperature and in situ pressure 100/150 MPa, followed by measurements at the constant confining effective pressure of 100/150 MPa over the temperature range of 20–600 °C. The intrinsic effects of temperature on velocities were hard to determine, due to thermal expansion and the consequent loosening of mineral structure. Figure 4a and Table 2 show the change of the P-wave velocities and $V_p$ anisotropy of the sample A as a function of pressure and temperature. The $V_p$ values of sample A increased from 5.24–6.25 km/s at 12 MPa to 5.65–6.43 km/s at 100 MPa. In the lower pressure range (up to 150 MPa), the increase rapid and non-linear. When the further increase, the increase in seismic wave is slight and linear in a frist approximation. Metamorphic rocks have been long been known to be mechanically anisotropic.

The seismic anisotropy itself is calculated as

$$A = \frac{V_{\max} - V_{\min}}{V_{mean}} \times 100\% \tag{13}$$

Seismic anisotropy is higher during the nonlinear part of the experiment and become relatively constantan during the linear part. The Vp velocity anisotropy shows an inverse behavior. It decreased towards higher pressure from 17.84% down to 12.95% (Fig. 4a, Table 2 in "Appendix"). The mean value of P-wave velocities of all samples increased as a function of pressure. The shear wave velocities

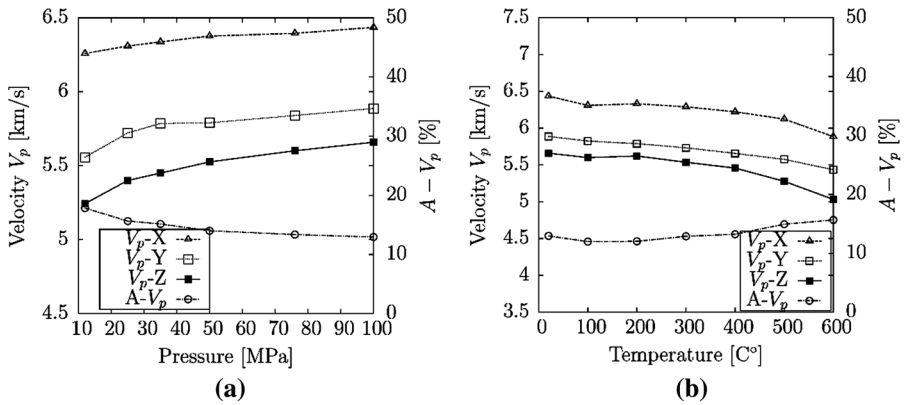


**Fig. 4** Seismic compressional wave (P) velocities as a function of pressure and temperature for sample A

showed a similar trend. The Vs values for the three directions of this sample were from 3.30–3.61 km/s at 12 MPa to 3.52–3.82 km/s at 100 MPa (see Fig. 4a, Table 2). In general, there is an increase in P- and S wave velocities with increasing pressure. In addition, P-wave velocities measured in three directions decreased with increasing temperature from 6.32–5.62 km/s at room temperature to 5.03–5.88 km/s at 600 °C. Furthermore, the velocity anisotropy (A-$V_p$%) shows an inverse behavior; it increases with higher temperature from 11.63% at room temperature to 15.56% at 600 °C (Fig. 4b, Table 2). In general, the P-wave velocities decreased and velocity anisotropy increased with increasing the temperature for both samples. The mean P-wave velocities of both samples increase from 3.87–4.60 km/s at 20 °C to 4.21–5.35 km/s at 600 °C. A similar behavior at increasing temperature was observed on the other samples. The S-wave velocities show a similar trend. Figure 5a, b show the Vs velocities of the sample A as a function of temperature. All three directional Vs velocities decreased from 3.80–3.60 km/s at room temperature to 3.63–3.49 km/s at 600 °C (Fig. 5b, Table 2).

### 4.2 Density

The densities of samples were calculated as a function of pressure and temperature with respect to P- and S wave velocities. The density of all samples increased from 2.75–2.93 g/cm$^3$ at 12 MPa to 2.76–2.96 g/cm$^3$ at 100 MPa (Fig. 6a, b and Table 2 in "Appendix"). Density of samples increases slightly and non-linearly with increasing pressure. On the other hand, at higher temperature, the density decreases because of thermal micro cracks. Figure 6a, b and Table 3 show the measured density of all samples as a function of pressure and temperature.

### 4.3 Deformation

Figure 7a, b and Table 3 show stress-deformation and temperature-deformation (thermal expansion) curve for all samples. Load and thermal induced deformation are measured in all six directions with the help of 12 strain measurement strain gauge. A substantial increase of stress as well as a compressed sample (deformation) is shown in Fig. 7a and b. In Fig. 7a and b, $e_1$, $e_2$, $e_3$, are the linear strains in X, Y, Z directions and Vol.-e is the volumetric strain of the sample. During the loading period where sample was compressed, we reported a compression as a positive value (see Fig. 7a, Table 3) and during thermal loading where sample was expanded, we reported expansion as a negative value (see Fig. 7b, Table 3) with a constant pressure of 100 MPa. The associate volumetric strains are shown in Fig. 7a and b. The stress–strain and thermal stress–strains curves non-linearly increase as a function of temperature and decrease as a function of pressure (see Fig. 7a, b, Table 3), this may be because of the same pressure and temperature applied in all six directions. Due to the high anisotropy nature of sample, it shows the non-linear behavior of stress-strain. Therefore, we did not find any post peak failure during testing.

### 4.4 Poisson's Ratio

The Poisson's ratio of rock sample is control by the P- and S wave velocities. Similarly, the Poisson's ratio of rock material is generally determined at the elastic stage (Shaocheng et al. 2018). Typical curves are shown for all samples in Fig. 8a, b and Table 2 as a function of pressure and temperature. The mean Poisson's ratio values of sample A decrease from 0.193 at 12 MPa to 0.184 at 100 MPa (Fig. 8a, b Table 3). The Poisson's ratio of sample A decreases with the increasing pressure. In contrast, the Poisson's ratio of sample B1 is almost constant with increasing the pressure but the value of Poisson's ratio of sample B2 increases with increasing the pressure. On the other hand, the Poisson's ratio of all samples decreases with the increasing thermal stress. For all rock types, the Poisson's ratio is more or less unaffected by temperature changes, and the minor variations (Fig. 8a and b) are random and can be considered as within the measurement uncertainty (Motra et al. 2013a, b, 2014a, b, c, 2016a, b, Motra and Wuttke 2016; Keitel et al. 2014).

### 4.5 Dynamic Elastic Moduli (Young's, Bulk, Shear Moduli)

Figure 9a, b and Table 3 show average curves for the Young's E, Bulk K and Shear μ moduli of the rock sample A as a function of pressure from 12 to 100 MPa and temperature from 20 to 600 °C. Deviations from the moduli occur with changes in the

Poisson's ratio (Shaocheng et al. 2018). This is due to the fundamental relationship between temperatures and due to the elastic equations depending on Vp- and Vs with the elastic, bulk, and shear moduli. Normally as increasing the pressure Poisson's is decreasing, on the other hand dynamic elastic moduli are increasing, which is shows in in Fig. 9a, b and Table 3. The dynamic moduli of all samples increase with the increase in pressure. Additionally, it is found that the moduli of metamorphic tested rock samples decreased with increasing temperature from 20 to 600 °C. It is apparent that temperature has a significant effect in decreasing these moduli properties. The mean density of all samples decreases with the increasing temperature.

## 5 Discussion

In this paper, the effects of pressure and temperature of rocks on their physical properties were discussed in detail. These are the irreversible changes that occur upon heating rocks to their room temperature. The effects of pressure and temperature are considered to be the irreversible changes that occur at increasing pressure and temperature. In metamorphic rocks, increasing pressure leads to increasing velocities and increasing temperature generally leads to decreasing velocities. The main causes of the velocity change are:

- The general increase of P- and S-wave velocities with increasing pressure is basically the result of the sample compaction, as is confirmed by the volumetric strain versus pressure (Fig. 7a, b and Tables 1 and 2) and density versus pressure curves (Fig. 6a, b and Table 2).
- Temperature dependence of the elastic properties of the rock-forming minerals and phase change of minerals;
- Temperature dependence of the elastic properties of the pore constituents and change of pore constituents (e.g., pore water) from a liquid to a gaseous state;
- Changes in the contact conditions at grains, crack boundaries, etc., resulting from variations of the interface effects and/or from different thermal expansion properties of rock-forming minerals.

Increase of velocity under the influence of pressure in the lower pressure range primarily is due to the closure of pores and micro-joints. This closure improves the contact between rock-forming minerals. At higher pressure, the compaction of the aggregate is nearly complete. Therefore, seismic wave velocities increase observed in loaded samples can be related to the overall damage of the materials. The decrease in elastic wave velocities with increased temperature could result in predicting higher porosities in using the time-average relationship, which is similar results in Kern et al. (1997), Motra and Wuttke (2016), D'Andrea et al. (1966), Deere and Miller (1965), Punturo et al. (2005), Moradian and Behnia (2009), Sarkar et al. (2012), Motra and Zertani (2018), Scheu et al. (2006) and Shaocheng et al. (2018). This is contradictory to some evidence that porosity tends to decrease with higher temperatures. In addition, as the seismic wave propagation is related to geomechanical properties of rocks, in particular to the elastic moduli, then the change in seismic wave velocities involves a change in geomechanical properties of rock. In Figs. 4, 5, 6, 7, 8 and 9 and Tables 2, 3, we see the change in seismic wave and basic geomechanical properties of rock during the loaded and thermally loaded conditions.

The velocity anisotropy can be linked to the texture of the samples. Those with a high anisotropy show a pronounced shape preferred orientation and sometimes, microcrystal in addition to layering within the groundmass of the sample.

The effect of temperature on elasticity and compressibility is substantially higher on the reservoir metamorphic rocks. Differences in mineral composition and lower porosity probably explain the differences in elastic, bulk and shear moduli, behavior with respect to temperature changes. The mechanical properties of rocks, calculation based on the analysis and using elastic wave data, were measured at high temperature. In general, elastic, bulk, shear moduli of the metamorphic rock samples decrease with the increasing temperature. However, all the laboratory tests be made at reservoir in situ temperature for the purpose of determining physical properties of rocks. These results confirm that the loaded and thermally induced micro cracks play an important role in the geomechanical properties of rocks.

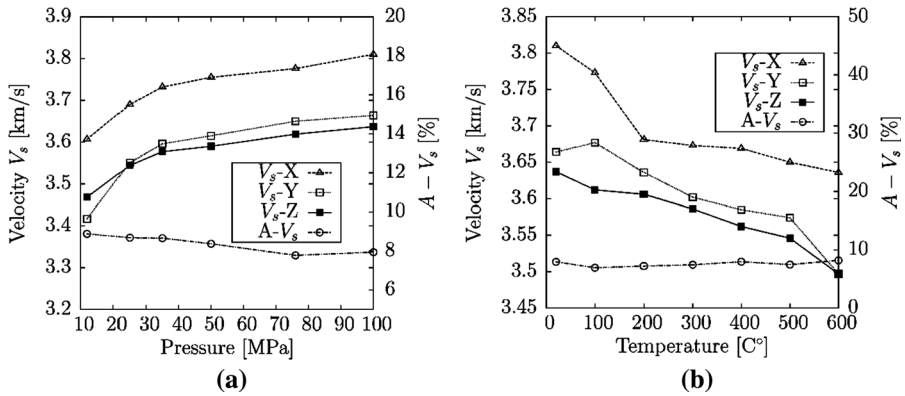


**Fig. 5** Seismic shear wave velocities (S) as a function of pressure and temperature for sample A

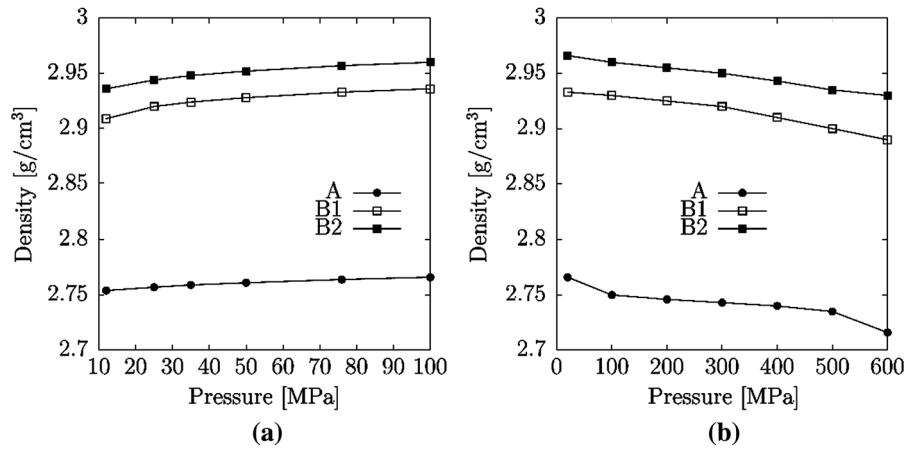


**Fig. 6** Density as a function of pressure and temperature for samples A, B1 and B2

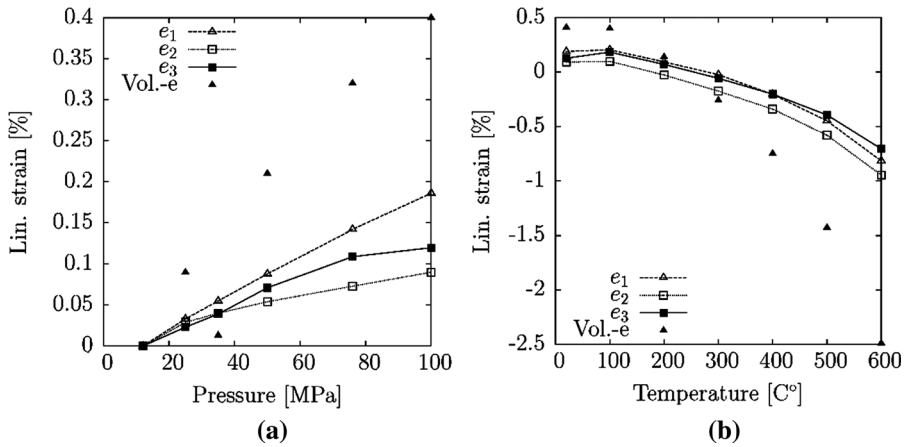


**Fig. 7** Linear and volumetric strain as a function of pressure and temperature for sample A

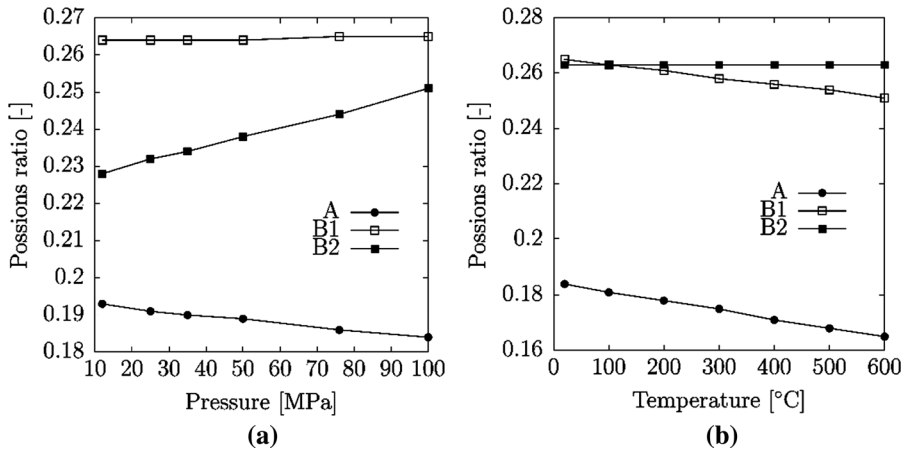


**Fig. 8** Poisson's ratio as function of pressure and temperature for samples A, B1 and B2

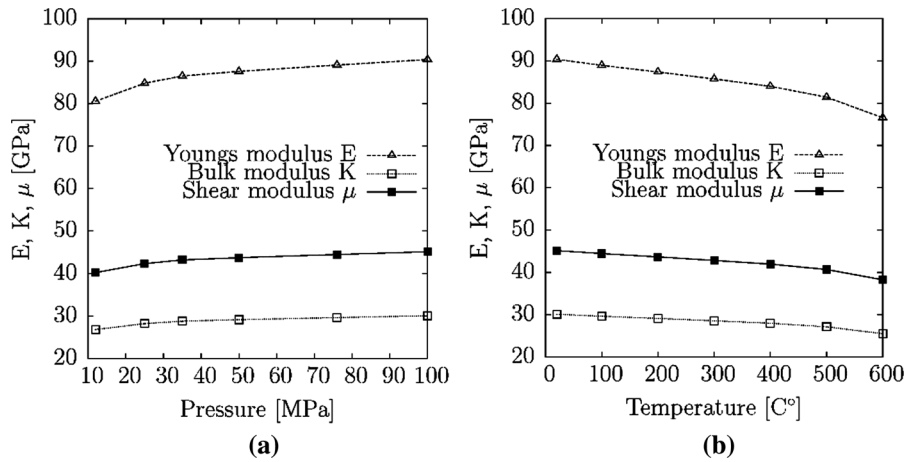


**Fig. 9** Dynamic elastic moduli as function of pressure and temperature for sample A

The presented data set of density, volumetric strain, Poisson's ratio, dynamic moduli show that there is a clear trend of increasing Poisson's ratio with increased as a function of pressure (Figs. 6, 7, 8, 9 and Table 2, 3).

The ratio of axial stress and resulting axial strain gives an elastic modulus characterizing the deformation behavior. Samples show an axial and a lateral deformation; relative change of dimension divided by relative change of axial length in stress direction is Poisson's ratio; it represents a second property characterizing the deformation behavior.

In reservoir area, when the heated water is contained, the rock of the around reservoir is subjected to compressed in situ stress and temperature increase. Above result shows that this stress induced and temperature rise cause development of crack and induce change in properties. Crack and change in properties can enhance the efficiency of the reservoir but can also affect the mechanical and physical behavior at different depths. The relationship between the Young's, bulk and shear moduli as well as density, Poisson's ratio and volumetric strain with elastic P- and S- wave velocities are valuable for understanding a metamorphic rock parameter evaluation. The data indicates strong correlation between these parameters. This paper considers that the presented dataset can help to reduce the risk reservoir drilling by an improving knowledge of the physical parameter in rock mass characterization. Therefore, a deeper

understanding of how mechanical parameters may influence the migration of fluid and change in mechanical parameter with respect to pressure and temperature is important. Knowledge of the mechanical properties at pressure and temperature of rock has become insincerely important with the wide-spread interest in physical process in underground rock mass. For meaningful analyses of mechanical properties, in addition to rock properties, their behavior in high pressure and temperature environment must be quantified. Some of these mechanical properties requiring knowledge of high pressure–temperature behavior of rock system include underground storage heat, disposal nuclear waste and geothermal reservoir evaluation.

## 6 Conclusion

In this study, basic geomechanical properties of three rock samples have been measured and analyzed in an integrated manner. Laboratory measurements have been carried out on the following physical parameters: compressional (P) and orthogonally polarized shear wave velocities ($S_1$, $S_2$) as a function of pressure and temperature using true triaxial multi-anvil apparatus.

The change in geomechanical properties influences the wave propagation through the sample as well as the behavior of wave generated, and therefore, needs a particular consideration. Seismic velocities increase with pressure due to compaction and first closing of micro cracks. The $V_p$ anisotropy decreases with pressure for same reason. Increasing the temperature, decreasing seismic wave velocities decrease but with increasing anisotropy. This behavior is found in most of the previous investigation also. This effect may be due to the opening of pore and micro-cracks during the expansion of sample by thermal stress. The density of metamorphic rock increases with the increasing pressure. Furthermore, the density of all investigated samples decreases with the increasing thermal stress.

Further, deformation in many cases can be approximated as a linear function of loading and thermal stress. Furthermore, it was found that pressure and temperature have a significant effect on the change of geomechanical properties of rocks. Seismic wave velocities can be used to measure various physical properties (density, deformation, Poisson's ratio, elastic moduli, and rock classification properties) on metamorphic rocks.

**Acknowledgements** This research is supported by EU H2020 project "Drilling in supercritical geothermal condition (DESCRAMBLE)", which is gratefully acknowledged by the authors. We thank ENEL Green Power for providing samples and for excellent cooperation.

## Appendix

See Tables 2, 3.

**Table 2** Summary of the elastic wave velocities, velocity anisotropy, Poisson's ratio and density as a function of pressure and temperature

| Sample | Pressure (MPa) | Temp. (°C) | Density (g/cm$^3$) | Poission ratio (−) | $V_p$ (km/s) | | | Mean Vp (km/s) | A-Vp (%) | $V_s$ (km/s) | | | Mean $V_s$ (km/s) | A-$V_s$ (%) |
|---|---|---|---|---|---|---|---|---|---|---|---|---|---|---|
| | | | | | X | Y | Z | | | X | Y | Z | | |
| A | 12 | 20 | 2.754 | 0.193 | 6.259 | 5.557 | 5.244 | 5.687 | 17.84 | 3.607 | 3.417 | 3.468 | 3.497 | 8.88 |
| | 25 | 20 | 2.757 | 0.191 | 6.309 | 5.722 | 5.400 | 5.810 | 15.65 | 3.690 | 3.551 | 3.544 | 3.595 | 8.68 |
| | 35 | 20 | 2.759 | 0.190 | 6.337 | 5.785 | 5.450 | 5.857 | 15.16 | 3.732 | 3.596 | 3.577 | 3.635 | 8.66 |
| | 50 | 20 | 2.761 | 0.189 | 6.376 | 5.790 | 5.526 | 5.897 | 14.40 | 3.755 | 3.615 | 3.590 | 3.653 | 8.37 |
| | 76 | 20 | 2.764 | 0.186 | 6.395 | 5.839 | 5.601 | 5.945 | 13.36 | 3.776 | 3.650 | 3.619 | 3.682 | 7.78 |
| | 100 | 20 | 2.766 | 0.184 | 6.435 | 5.887 | 5.659 | 5.994 | 12.95 | 3.810 | 3.664 | 3.637 | 3.703 | 7.94 |
| | 100 | 100 | 2.750 | 0.181 | 6.308 | 5.825 | 5.600 | 5.911 | 11.97 | 3.773 | 3.677 | 3.612 | 3.687 | 6.93 |
| | 100 | 200 | 2.460 | 0.178 | 6.331 | 5.789 | 5.621 | 5.913 | 12.02 | 3.681 | 3.636 | 3.606 | 3.641 | 7.21 |
| | 100 | 300 | 2.743 | 0.175 | 6.289 | 5.732 | 5.536 | 5.852 | 12.88 | 3.673 | 3.602 | 3.586 | 3.620 | 7.43 |
| | 100 | 400 | 2.740 | 0.171 | 6.222 | 5.657 | 5.457 | 5.779 | 13.23 | 3.669 | 3.585 | 3.562 | 3.605 | 7.96 |
| | 100 | 500 | 2.735 | 0.168 | 6.122 | 5.576 | 5.277 | 5.658 | 14.94 | 3.650 | 3.574 | 3.546 | 3.590 | 7.47 |
| | 100 | 600 | 2.716 | 0.165 | 5.885 | 5.435 | 5.032 | 5.451 | 15.66 | 3.636 | 3.497 | 3.497 | 3.543 | 8.19 |
| B1 | 12 | 20 | 2.909 | 0.264 | 4.884 | 4.631 | 3.611 | 4.375 | 29.08 | 2.627 | 2.584 | 2.325 | 2.512 | 20.24 |
| | 25 | 20 | 2.920 | 0.264 | 5.218 | 4.872 | 3.760 | 4.617 | 31.56 | 2.724 | 2.665 | 2.434 | 2.608 | 18.48 |
| | 35 | 20 | 2.924 | 0.264 | 5.491 | 5.132 | 3.860 | 4.828 | 33.79 | 2.819 | 2.806 | 2.498 | 2.707 | 20.26 |
| | 50 | 20 | 2.928 | 0.264 | 5.782 | 5.583 | 3.946 | 5.104 | 35.98 | 2.991 | 2.974 | 2.694 | 2.886 | 20.83 |
| | 76 | 20 | 2.933 | 0.265 | 6.226 | 6.028 | 4.256 | 5.503 | 35.79 | 3.157 | 3.165 | 2.849 | 3.057 | 22.73 |
| | 100 | 20 | 2.936 | 0.265 | 6.407 | 6.183 | 4.608 | 5.732 | 31.38 | 3.237 | 3.440 | 2.915 | 3.197 | 27.83 |
| | 100 | 100 | 2.930 | 0.263 | 6.395 | 6.095 | 4.590 | 5.693 | 31.70 | 3.334 | 3.306 | 2.984 | 3.208 | 20.18 |
| | 100 | 200 | 2.925 | 0.261 | 6.273 | 6.000 | 4.620 | 5.631 | 29.35 | 3.340 | 3.295 | 3.019 | 3.218 | 18.10 |
| | 100 | 300 | 2.920 | 0.258 | 6.288 | 5.993 | 4.600 | 5.627 | 30.01 | 3.310 | 3.300 | 3.026 | 3.212 | 18.46 |
| | 100 | 400 | 2.910 | 0.256 | 6.361 | 6.034 | 4.468 | 5.621 | 33.68 | 3.295 | 3.298 | 3.020 | 3.204 | 19.50 |
| | 100 | 500 | 2.900 | 0.254 | 6.322 | 6.039 | 4.450 | 5.604 | 33.39 | 3.278 | 3.278 | 3.033 | 3.196 | 18.55 |
| | 100 | 600 | 2.890 | 0.251 | 6.351 | 5.969 | 4.483 | 5.601 | 33.35 | 3.275 | 3.260 | 3.018 | 3.184 | 17.04 |

**Table 2** continued

| Sample | Pressure (MPa) | Temp. (°C) | Density (g/cm$^3$) | Poission ratio (−) | $V_p$ (km/s) | | | Mean Vp (km/s) | A-Vp (%) | $V_s$ (km/s) | | | Mean $V_s$ (km/s) | A-$V_s$ (%) |
|---|---|---|---|---|---|---|---|---|---|---|---|---|---|---|
| | | | | | X | Y | Z | | | X | Y | Z | | |
| B2 | 12 | 20 | 2.936 | 0.228 | 4.901 | 4.626 | 2.767 | 4.407 | 52.06 | 2.66 | 2.528585 | 2.26 | 2.481 | 25.76 |
| | 25 | 20 | 2.944 | 0.232 | 5.375 | 4.998 | 3.308 | 4.589 | 45.32 | 2.81 | 2.735383 | 2.51 | 2.686 | 21.10 |
| | 35 | 20 | 2.948 | 0.234 | 5.625 | 5.209 | 3.597 | 4.718 | 42.16 | 2.94 | 2.86046 | 2.65 | 2.816 | 18.37 |
| | 50 | 20 | 2.952 | 0.238 | 5.883 | 5.469 | 3.974 | 4.926 | 37.36 | 3.1 | 2.998328 | 2.79 | 2.961 | 18.33 |
| | 76 | 20 | 2.957 | 0.244 | 6.051 | 5.740 | 4.448 | 5.263 | 29.62 | 3.24 | 3.200257 | 3 | 3.148 | 14.15 |
| | 100 | 20 | 2.960 | 0.251 | 6.378 | 5.990 | 4.793 | 5.600 | 27.70 | 3.32 | 3.296789 | 3.13 | 3.248 | 12.58 |
| | 150 | 20 | 2.966 | 0.263 | 6.672 | 6.304 | 5.291 | 6.276 | 22.69 | 3.48 | 3.481391 | 3.32 | 3.425 | 10.45 |
| | 150 | 100 | 2.960 | 0.263 | 6.601 | 6.424 | 5.426 | 6.279 | 19.11 | 3.61 | 3.565079 | 3.39 | 3.521 | 11.62 |
| | 150 | 200 | 2.955 | 0.263 | 6.770 | 6.500 | 5.558 | 6.277 | 19.31 | 3.72 | 3.656434 | 3.48 | 3.620 | 12.18 |
| | 150 | 300 | 2.950 | 0.263 | 6.837 | 6.667 | 5.703 | 6.274 | 17.72 | 3.69 | 3.679277 | 3.52 | 3.630 | 9.05 |
| | 150 | 400 | 2.943 | 0.263 | 6.831 | 6.715 | 5.748 | 6.271 | 16.84 | 3.69 | 3.694707 | 3.54 | 3.642 | 9.03 |
| | 150 | 500 | 2.935 | 0.263 | 6.978 | 6.679 | 5.771 | 6.267 | 18.64 | 3.75 | 3.695009 | 3.53 | 3.659 | 10.67 |
| | 150 | 600 | 2.93 | 0.263 | 6.996 | 6.686 | 5.805 | 6.261 | 18.33 | 3.81 | 3.713465 | 3.53 | 3.683 | 11.04 |

**Table 3** Summary of the elastic wave velocities, density, Poisson's ratio axial and volumetric deformation and dynamic elastic moduli as a function of pressure and pressure

| Sample | Pressure (MPa) | Temp. (°C) | Density (g/cm$^3$) | Mean $V_p$ (km/s) | Mean $V_s$ (km/s) | Poisson's ratio (−) | Axial strain (%) | Voil. strain (%) | Young's modulus (GPa) | Bulk modulus (GPa) | Shear modulus (GPa) |
|---|---|---|---|---|---|---|---|---|---|---|---|
| A | 12 | 20 | 2.754 | 5.687 | 3.497 | 0.193 | 0.00 | − 0.03 | 80.574 | 43.681 | 33.782 |
| | 25 | 20 | 2.757 | 5.810 | 3.595 | 0.191 | 0.09 | 0.09 | 84.808 | 45.779 | 35.597 |
| | 35 | 20 | 2.759 | 5.857 | 3.635 | 0.190 | 0.13 | 0.13 | 86.525 | 46.561 | 36.346 |
| | 50 | 20 | 2.761 | 5.897 | 3.653 | 0.189 | 0.21 | 0.21 | 87.606 | 46.905 | 36.849 |
| | 76 | 20 | 2.764 | 5.945 | 3.682 | 0.186 | 0.32 | 0.32 | 89.085 | 47.315 | 37.551 |
| | 100 | 20 | 2.766 | 5.994 | 3.703 | 0.184 | 0.40 | 0.40 | 90.386 | 47.630 | 38.179 |
| | 100 | 100 | 2.750 | 5.911 | 3.687 | 0.181 | − 0.35 | 0.49 | 88.954 | 46.487 | 37.658 |
| | 100 | 200 | 2.746 | 5.913 | 3.641 | 0.178 | − 0.74 | 0.14 | 87.390 | 45.207 | 37.098 |
| | 100 | 300 | 2.743 | 5.852 | 3.620 | 0.175 | − 1.23 | − 0.26 | 85.728 | 43.901 | 36.494 |
| | 100 | 400 | 2.740 | 5.779 | 3.605 | 0.171 | − 1.91 | − 0.75 | 83.986 | 42.586 | 35.851 |
| | 100 | 500 | 2.735 | 5.658 | 3.590 | 0.168 | − 2.96 | − 1.43 | 81.439 | 40.888 | 34.862 |
| | 100 | 600 | 2.716 | 5.451 | 3.543 | 0.165 | − 2.96 | − 2.49 | 76.549 | 38.066 | 32.858 |
| B1 | 12 | 20 | 2.909 | 4.375 | 2.512 | 0.264 | 0.00 | − 0.03 | 46.041 | 32.498 | 18.214 |
| | 25 | 20 | 2.920 | 4.617 | 2.608 | 0.264 | 0.38 | 0.38 | 50.269 | 35.509 | 19.884 |
| | 35 | 20 | 2.924 | 4.828 | 2.707 | 0.264 | 0.51 | 0.51 | 54.469 | 38.498 | 21.543 |
| | 50 | 20 | 2.928 | 5.104 | 2.886 | 0.264 | 0.64 | 0.64 | 61.709 | 43.648 | 24.403 |
| | 76 | 20 | 2.933 | 5.503 | 3.057 | 0.265 | 0.81 | 0.81 | 70.007 | 49.587 | 27.677 |
| | 100 | 20 | 2.936 | 5.732 | 3.197 | 0.265 | 0.92 | 0.92 | 76.493 | 54.261 | 30.233 |
| | 100 | 100 | 2.930 | 5.693 | 3.208 | 0.263 | − 0.03 | 1.98 | 77.429 | 54.490 | 30.649 |
| | 100 | 200 | 2.925 | 5.631 | 3.218 | 0.261 | − 0.07 | 0.87 | 76.442 | 53.267 | 30.315 |
| | 100 | 300 | 2.920 | 5.627 | 3.212 | 0.258 | − 0.36 | 0.59 | 75.991 | 52.435 | 30.192 |
| | 100 | 400 | 2.910 | 5.621 | 3.204 | 0.256 | − 0.67 | 0.27 | 75.440 | 51.554 | 30.029 |
| | 100 | 500 | 2.900 | 5.604 | 3.196 | 0.254 | − 1.03 | − 0.09 | 74.775 | 50.614 | 29.820 |
| | 100 | 600 | 2.890 | 5.601 | 3.184 | 0.251 | − 1.55 | − 0.60 | 73.957 | 49.587 | 29.549 |
| B2 | 12 | 20 | 2.936 | 4.407 | 2.481 | 0.228 | 0.000 | − 0.026 | 43.758 | 26.853 | 17.810 |
| | 25 | 20 | 2.944 | 4.589 | 2.686 | 0.232 | 0.083 | 0.249 | 52.438 | 32.583 | 21.286 |
| | 35 | 20 | 2.948 | 4.718 | 2.816 | 0.234 | 0.124 | 0.370 | 57.940 | 36.329 | 23.473 |
| | 50 | 20 | 2.952 | 4.926 | 2.961 | 0.238 | 0.173 | 0.518 | 64.571 | 41.083 | 26.078 |
| | 76 | 20 | 2.957 | 5.263 | 3.148 | 0.244 | 0.225 | 0.673 | 72.920 | 47.532 | 29.301 |
| | 100 | 20 | 2.960 | 5.600 | 3.248 | 0.251 | 0.264 | 0.791 | 78.817 | 52.669 | 31.512 |
| | 150 | 20 | 2.966 | 6.276 | 3.425 | 0.263 | 0.321 | 0.961 | 88.246 | 62.097 | 34.931 |
| | 150 | 100 | 2.960 | 6.279 | 3.521 | 0.263 | − 0.008 | 1.226 | 92.621 | 65.194 | 36.661 |
| | 150 | 200 | 2.955 | 6.277 | 3.620 | 0.263 | − 0.028 | 1.068 | 97.329 | 68.495 | 38.526 |
| | 150 | 300 | 2.950 | 6.274 | 3.630 | 0.263 | − 0.052 | 0.829 | 98.589 | 69.368 | 39.026 |
| | 150 | 400 | 2.943 | 6.271 | 3.642 | 0.263 | − 0.139 | 0.570 | 99.030 | 69.660 | 39.202 |
| | 150 | 500 | 2.935 | 6.267 | 3.659 | 0.263 | − 0.252 | 0.231 | 99.765 | 70.154 | 39.496 |
| | 150 | 600 | 2.930 | 6.261 | 3.683 | 0.263 | − 0.414 | − 0.254 | 100.387 | 70.558 | 39.746 |

## References


D'Andrea DV, Fischer RL, Fogelson DE (1966a) Prediction of compressive strength from other rock properties, vol 6702. Report of investigations. US Bureau of Mines, Washington

D'Andrea DV, Fischer RL, Fogelson DE (1966b) Prediction of compressive strength from other rock properties, vol 6702. Report of investigations. US Bureau of Mines, Washington, p 1995

Deere DU, Miller RP (1965) Engineering classification and index properties for intact rock. Technical report AFWL-TR-65-116. US Air Force Weapons Laboratory, Kirtland Base, NM

Gebrande H, Kern H, Rummel F (1982) Elasticity and inelasticity. In: Hellwege K-H (ed) Landolt-Börnstein. numerical data and functional relationships in science and technology. New series; group V. geophysics and space research. Vol. 1b: physical properties of rocks. Springer, Berlin, pp 1–233

Hajpál M, Török A (2004) Mineralogical and colour changes of quartz sandstones by heat. Environ Geol 46:311–322

Keitel K, Jung B, Motra HB, Stutz H (2014) Quality assessment of coupled partial models considering soil-structure coupling. Eng Struct 59:565–573

Kern H (1978) H. The effect of high temperature and high confining pressure on compressional wave velocities in quartz-bearing and quartz-free igneous and metamorphic rocks. Tectonophysics 44:185–203

Kern H, Liu B, Popp T (1997) Relationship between anisotropy of P and S wave velocities and anisotropy of attenuation in serpentinite and amphibolite. J Geophys Res [Solid Earth] 102(B2):3051–3065

Kern H, Popp T, Gorbatsevich F, Zharikov A, Lobanov KV, Smirnov YP (2001) Pressure and temperature dependence VP and VS in rocks from the superdeep well and from the surface analogues at Kola and the nature of velocity anisotropy. Tectonophysics 338:113–134

Lama RD, Vutukuri VS (1978) Handbook on mechanical properties of rocks, vol II. Trans Tech Publications, Clausthal

Liu X, Zhang C, Yuan S, Fityus S, William Sloan S, Buzzi O (2016) Effect of high temperature on mineralogy, microstructure, shear stiffness and tensile strength of two Australian mudstones. Rock Mech Rock Eng. https://doi.org/10.1007/s00603-016-1024-y

Moradian ZA, Behnia M (2009a) Predicting the uniaxial compressive strength and static Young's modulus of intact sedimentary rocks using the ultrasonic test. Int J Geomech 9:1–14

Moradian ZA, Behnia M (2009b) Predicting the uniaxial compressive strength and static Young's modulus of intact sedimentary rocks using the ultrasonic test. Int J Geomech 9:1e14

Motra HB, Wuttke F (2016) Temperature dependence of elastic P- and S-wave properties of rocks: applications to geothermal reservoir evaluation. In: Energy Geotechnics—proceedings of the 1st international conference on energy geotechnics, ICEGT 2016, Kiel, 29–31 Aug 2016, ISBN 9781138032996, pp 311–316

Motra HB, Wuttke F (2016) Temperature dependence of elastic P- and S-wave properties of rocks: applications to geothermal reservoir evaluation. In: Energy geotechnics—proceedings of the 1st international conference on energy geotechnics, ICEGT

Motra HB, Zertani Z (2018) Influence of loading and heating processes on elastic and geomechanical properties of eclogites and granulites. J Rock Mech Geotech Eng 10:127–137

Motra HB, Dimmig-Osburg A, Hildebrand J (2013) Influence of measurement uncertainties on results of creep prediction of concrete under cyclic loading. In: Proceedings of the 8th international conference on fracture mechanics of concrete and concrete structures, FraMCoS

Motra HB, Osburg AD, Hildebrand J (2013) Uncertainty quantification on creep deflection of concrete beam subjected to cyclic loading. In: Safety, reliability, risk and life-cycle performance of structures and infrastructures—proceedings of the 11th international conference on structural safety and reliability, ICOSSAR

Motra HB, Hildebrand J, Dimmig-Osburg A (2014a) Influence of specimen dimensions and orientations on the tensile properties of structural steel. Materialpruefung/Mater Test 56(11–12):929–936

Motra HB, Dimmig-Osburg A, Hildebrand J (2014b) Quality assessment of models with an application to cyclic creep prediction of concrete. Int J Reliab Saf 8(2):262–283

Motra HB, Hildebrand J, Dimmig-Osburg A (2014c) Assessment of strain measurement techniques to characterize mechanical properties of structural steel. Int J Eng Sci Technol 17:260–269

Motra HB, Hildebrand J, Wuttke F (2016a) Monte Carlo method for the evaluation of measurement uncertainty: application to determine material properties. Probab Eng Mech 45:220–228

Motra HB, Stutz H, Wuttke F (2016b) Quality assessment of soil bearing capacity factor models of shallow foundations. Soils Found 56(2):265–276

Nye JF (1985) Physical properties of crystals—their representation by tensors and matrices. Oxford University Press, UK

Punturo R, Kern H, Cirrincione R, Mazzoleni P, Pezzino A (2005a) P-and S-wave velocities and densities in silicate and calcite rocks from the Peloritani Mountains Sicily (Italy): the effect of pressure, temperature and the direction of wave propagation. Tectonophysics 409:55–72

Punturo R, Kern H, Cirrincione R, Mazzoleni P, Pezzino A (2005b) P-and S-wave velocities and densities in silicate and calcite rocks from the Peloritani Mountains Sicily (Italy): the effect of pressure, temperature and the direction of wave propagation. Tectonophysics 409:55e72

Sarkar K, Vishal V, Sign TN (2012a) An empirical correlation of index geomechanical parameters with the compressional wave velocity. Geotech Geol Eng 30:469–479

Sarkar K, Vishal V, Sign TN (2012b) An empirical correlation of index geomechanical parameters with the compressional wave velocity. Geotech Geol Eng 30:469e79

Scheu B, Kern H, Spieler O, Dingwell DB (2006) Temperature dependence of elastic P- and S-wave velocities in porous Mt. Unzen dacite J Volcanol Geoth Res 153:136–147

Schön JH (2011) Physical properties of rocks: a workbook. Elsevier, Amsterdam

Shaocheng J, Le L, Motra HB, Wuttke F, Michibayashi K, Salisbury MH (2018) Poisson's ratio and auxetic properties of natural rocks. J Geophys Res Solid Earth 123:1161–1185

Smorodinov MI, Motovilove EA, Volkov VA (1970) Determination of correlation relationships between strength and some physical characteristics of rocks. Proc Int Soc Rock Mech 1:1–19

Tian H, Kempka T, Xu NX, Ziegler M (2012) Physical properties of sandstones after high temperature treatment. Rock Mech Rock Eng 45:1113–1117

Tian H, Kempka T, Xu NX, Ziegler M (2013) A modified Mohr–Coulomb failure criterion for intact granites exposed to high temperatures. Springer Series in geomechanics and geoengineering. Springer, Berlin, pp 379–393

Youash Y (1970) Dynamic physical properties of rocks: part 2, experimental result. In: Proceedings of the 2nd congress of the international society for rock mechanics, Beograd, 21–26 Sept 1970. Institute for Development of Water Resources, Beograd, pp 185–195